Journal of Solid State Chemistry **159,** 328–335 (2001)
doi:10.1006/jssc.2001.9165, available online at http://www.idealibrary.com on IDEAL®

Three-Dimensional Bimetallic Ferrimagnets $[Mn(L)]_3[Cr(CN)_6]_2 \cdot nH_2O$ (L = ethylenediamine, $n = 4$; L = glycine amide, $n = 2.5$) and Relevance to a Prussian Blue Analogue $Mn_3[Cr(CN)_6]_2 \cdot 12H_2O$

Naoki Usuki, Mitsuteru Yamada, Masaaki Ohba, and Hisashi Ōkawa[1]

Department of Chemistry, Faculty of Science, Kyushu University, Hakozaki, Higashiku 6-10-1, Fukuoka, Japan
E-mail: okawascc@mbox.nc.kyushu-u.ac.jp

Received March 20, 2001; accepted March 21, 2001

IN DEDICATION TO THE LATE PROFESSOR OLIVIER KAHN FOR HIS PIONEERING CONTRIBUTIONS TO THE FIELD OF MOLECULAR MAGNETISM

Two cyanide-bridged bimetallic assemblies, $[Mn(en)]_3[Cr(CN)_6]_2 \cdot 4H_2O$ (1) (en = ethylenediamine) and $[Mn(glya)]_3[Cr(CN)_6]_2 \cdot 2.5H_2O$ (2) (glya = glycine amide), have been obtained. X-ray crystallographic studies indicate that they have a three-dimensional network structure based on a defective cubane unit. Magnetic studies demonstrate that both are ferrimanget with $T_c = 69$ K for 1 and 71 K for 2. Remnant magnetizations for 1 and 2 are 1.2×10^4 and 1.1×10^4 cm^3 G mol^{-1}, respectively, and coercive fields are 28 and 19 G, respectively. The assemblies 1 and 2 are relevant to a Prussian blue analogue, $Mn_3[Cr(CN)_6]_2 \cdot 12H_2O$, which is also a ferrimagnet with $T_c = 63$ K, a remnant magnetization of 3.1×10^3 cm^3 G mol^{-1} and a coercive field of 8 G.

Key Words: **bimetallic assembly; ferrimagnet; Prussian blue; three-dimensional network; defective cubane.**

INTRODUCTION

Recently, there has been increasing interest in metal assemblies of an ordered network with the aim of providing magnetic materials exhibiting spontaneous magnetization (1–11). Prussian Blue compounds form a family of magnetic materials and a high magnetic phase transition temperature has been observed for some of them: $CsMn^{II}[Cr^{III}(CN)_6]$ ($T_c = 90$ K) (12), $CsNi^{II}[Cr^{III}(CN)_6]$ ($T_N = 90$ K) (13), $Cs_2Mn^{II}[V^{II}(CN)_6]$ ($T_N = 125$ K) (14), $Cs_{0.75}Cr^{II}_{1.125}[Cr^{III}(CN)_6]$ ($T_N = 190$ K) (15), $Cr^{II}_3[Cr^{III}(CN)_6]_2 \cdot 10H_2O$ ($T_N = 240$ K) (16), $V[Cr(CN)_6]_{0.86} \cdot 2.8H_2O$ ($T_c = 315$ K) (17). However, the magnetostructural correlation for Prussian Blue compounds is still unclear because of the lack of detailed structural infomation.

We have studied magnetic properties of bimetallic assemblies derived from $[M(CN)_6]^{3-}$ and planar $[Ni^{II}(diamine)]^{2+}$ (18). They include $PPh_4[Ni(pn)_2][M(CN)_6] \cdot H_2O$ (pn = 1,2-propanediamine, $M = Cr^{III}$, Fe^{III}, Co^{III}) of a one-dimensional zig-zag chain structure, $[Ni(en)_2]_3[M(CN)_6]_2 \cdot 2H_2O$ ($M = Cr^{III}$, Mn^{III}, Fe^{III}, Co^{III}) of a one-dimensional rope-ladder structure, $[Ni(N\text{-men})_2]_3[M(CN)_6]_2 \cdot 15H_2O$ (N-men = N-methylethylenediamine, $M = Fe^{III}$, Co^{III}) of a two-dimensional honeycomb sheet structure, and $[Ni(L)_2]_2[Fe(CN)_6]X \cdot nH_2O$ (L = en, pn, 1,1-dimethylethylendiamine) of a square sheet structure. An important conclusion drawn from the magnetic studies for those bimetallic assemblies is that spontaneous magnetization occurs only in the two-dimensional network structures. This fact strongly suggests that a three-dimensional network is important for achieving a high magnetic ordering temperature. The first three-dimensional bimetallic assemblies based on a cubane unit, $[Ni(L)_2]_3[Fe(CN)_6]X_2$ (L = en or tn (trimethylenediamine); $X = ClO_4^-$ or PF_6^-), have been synthesized in our laboratory, but they show no magnetic ordering because of the diamagnetic nature of $[Fe^{II}(CN)_6]^{4-}$ (19).

In order to construct a three-dimensional bimetallic network based on $[M(CN)_6]^{3-}$ as the bridging constituent, the second metal complex as the connector must prepare at least three vacant sites for accepting cyanide nitrogens from adjacent $[M(CN)_6]^{3-}$ ions. Such a structural requirement about the connector metal is successfully effected in $[Mn(en)]_3[Cr(CN)_6]_2 \cdot 4H_2O$ (**1**) (en = ethylenediamine) and $[Mn(glya)]_3[Cr(CN)_6]_2 \cdot 2.5H_2O$ (**2**) (glya = glycine amide), which is obtained by the reaction of stoichiometric amounts of Mn^{II} chloride, the supporting ligand (en or glya), and $K_3[Cr(CN)_6]$ in water. They have a three-dimensional network structure based on a defective cubane unit and show a ferrimagnetic ordering with a considerably high T_c. The structural relevance of **1** and **2** to a Prussian Blue analogue, $Mn_3[Cr(CN)_6]_2 \cdot 12H_2O$ (**3**), is also reported.

[1] To whom correspondence should be addressed.

0022-4596/01 $35.00

EXPERIMENTAL

Physical measurements. Elemental analyses of carbon, hydrogen, and nitrogen were obtained at the Service Center for Elemental Analysis at Kyushu University. Metal (Cr and Mn) analyses were made on a Shimadzu AA-680 Atomic Absorption/Flame Emission Spectrophotometer. Infrared spectra were measured on KBr disks with a Perkin–Elmer Spectrum BX FT-IR system. Magnetic susceptibilities were measured on a Quantum Design MPMS XL SQUID susceptometer. Data were corrected for the magnetization of the sample holder and capsule used. Diamagnetic corrections were made with Pascal's constants. Effective magnetic moments were calculated by the equation $\mu_{\text{eff}} = 2.828(\chi_M T)^{1/2}$, where χ_M is the molar magnetic susceptibility corrected for diamagnetism of the constituting atoms. Field dependences of magnetization were determined under an applied magnetic field of 50 kG.

Preparations. The syntheses of **1** and **2** were carried out under anaerobic conditions to avoid oxidation by atmospheric dioxygen.

$[Mn(en)]_3[Cr(CN)_6]_2 \cdot 4H_2O$ (**1**). $MnCl_2 \cdot 4H_2O$ (120 mg, 0.6 mmol) was dissolved in deoxygenated water (10 cm^3). To this solution were added an aqueous solution (10 cm^3) of ethylenediamine (36 mg, 0.6 mmol) and an aqueous solution (10 cm^3) of $K_3[Cr(CN)_6]$ (140 mg, 0.4 mmol), and the resulting turbid mixture was allowed to stand for few days to obtain pale green cubic crystals. The crystals were separated by suction filtration, washed with water, and dried in air. Anal. Found (%): C, 25.92; H, 3.74; N, 30.20; Mn, 19.49; Cr, 12.19. Calcd. (%) for $C_{18}H_{32}N_{18}O_4Mn_3Cr_2$: C, 25.94; H, 3.87; N, 30.25; Mn, 19.78; Cr, 12.48. IR (cm^{-1}, KBr disk): 3368, 3305, 2972, 2895, 2152, 1592, 1463.

$[Mn(glya)]_3[Cr(CN)_6]_2 \cdot 2.5H_2O$ (**2**). To the solution of $MnCl_2 \cdot 4H_2O$ (120 mg, 0.6 mmol) in deoxygenated water (10 cm^3), an aqueous solution (10 cm^3) of glya · HCl (70 mg, 0.6 mmol) and KOH (35 mg, 0.6 mmol) and an aqueous solution (10 cm^3) of $K_3[Cr(CN)_6]$ (140 mg, 0.4 mmol) were added. The resulting turbid mixture was allowed to stand for a few days to obtain pale green cubic crystals. They were separated, washed with water, and dried in air. Anal. Found (%): C, 25.45; H, 2.65; N, 29.69; Mn, 19.41; Cr, 12.15. Calcd. (%) for $C_{18}H_{23}N_{18}O_{5.5}Mn_3Cr_2$: C, 25.22; H, 2.82; N, 29.41; Mn, 19.22; Cr, 12.13. IR (cm^{-1}, KBr disk): [$\nu_{C\equiv N}$] 3501, 3428, 3374, 3323, 2152, 1678, 1591.

$Mn_3[Cr(CN)_6]_2 \cdot 12H_2O$ (**3**). This complex was prepared as a pale green microcrystalline powder by the literature method (21). Anal. Found (%): C, 17.87; H, 3.15; N, 21.10; Mn, 19.61; Cr, 12.50. Calcd. (%) for $C_{12}H_{24}N_{12}O_{12}Mn_3Cr_2$: C, 18.08; H, 3.03; N, 21.08; Mn, 20.67; Cr, 13.04. IR (cm^{-1}, KBr disk): 2160.

X-ray crystallography. Each single crystal of **1** and **2** was sealed in a glass capillary and used for crystallographic measurements at -30°C on a Rigaku AFC7R diffractometer, with graphite-monochromated MoK_α radiation ($\lambda = 0.71069$ Å) and a 12-kW rotating anode generator. The cell constant and an orientation matrix for the data collection were obtained from 25 reflections, and the ω–2θ scan mode was used for the intensity corrections at -30 ± 1°C. The octant measured was $\pm h$, $+k$, $+l$ for both complexes. Pertinent crystallographic parameters are summarized in Table 1.

TABLE 1
Crystal Parameters for 1 and 2

	Compound		
	1	**1**	**2**
Formula	$C_{18}H_{32}N_{18}Cr_2Mn_3O_4$	$C_{18}H_{32}N_{18}Cr_2Mn_3O_4$	$C_{18}H_{23}N_{18}Cr_2Mn_3O_{5.5}$
Formula weight	833.37	833.37	848.30
Crystal color	Pale green	Pale green	Pale green
Temperature (°C)	23	-30	-30
Crystal system	Monoclinic	Monoclinic	Monoclinic
Sapce group	$C2/c$ (#15)	$C2/c$ (#15)	$C2/c$ (#15)
a (Å)	24.505(7)	24.485(5)	24.569(3)
b (Å)	11.323(4)	11.295(4)	11.605(2)
c (Å)	14.810(4)	14.768(5)	14.328(2)
β (°)	120.69(2)	120.68(2)	121.177(8)
V (Å^3)	3533(1)	3512(1)	3495.0(8)
Z	4	4	4
D_c (g cm^{-3})	1.566	1.557	1.612
No. observations ($I > 3.00\sigma(I)$)	3032	2948	3127
R	0.033	0.032	0.036
R_w	0.042	0.038	0.052

The intensities of the representative reflections were measured after every 150 measurements, and over the course of the data collection the standards decreased by 5.5% for **1** and increased by 1.0% for **2**. A linear correction factor was applied to the data to account for the decay phenomena observed. Intensity data were corrected for Lorentz and polarization effects.

The structures were solved by a direct method and expanded using Fourier techniques. The nonhydrogen atoms were refined anisotropically. The hydrogen atoms were included in the structure factor calculations but not refined. All calculations were carried out on an IRIS O_2 computer using the teXsan crystallographic software package from the Molecular Structure Corporation (22).

RESULTS AND DISCUSSION

Preparation and general characterization. The bimetallic assemblies **1** and **2** were obtained as good crystals by the reaction of Mn^{II} chloride, the supporting ligand (en or glya), and $K_3[Cr(CN)_6]$ in the 3:3:2 molar ratio in water. All synthetic operations were carried out under nitrogen using a Schlenk apparatus in order to avoid oxidation by dioxygen. The bimetallic assemblies were found to be stable against dioxygen. It is generally considered that amine nitrogen has a low affinity toward Mn^{II}, but the coordination of en and glya to Mn^{II} through their amine nitrogen is evidently confirmed by X-ray crystallography as will be disucussed later. The IR spectrum of **2** shows the ν(CO) vibration of glya at 1678 cm^{-1}, which is low relative to 1687 cm^{-1}, of glya · HCl. This fact suggests that the glya is bonded to the Mn through the amide oxygen. The IR spectra of **1** and **2** have one ν(CN) band at 2152 cm^{-1} that is high in frequency relative to the ν(CN) band of $K_3[Cr(CN)_6]$ (2131 cm^{-1}). This fact means that all the cyanide groups of $[Cr(CN)_6]^{3-}$ are involved in the bridge to adjacent Mn^{II} ions. Complex **1** shows ν_{as}(NH) and ν_s(NH) vibrations at 3368 and 3305 cm^{-1}, respectively. Complex **2** shows four IR bands attributable to the N–H stretching vibrations of the amine (–CH_2NH_2) and amide (–CO–NH_2) groups.

Crystal structures. The structure of $[Mn(glya)]_3[Cr(CN)_6]_2 \cdot 2.5H_2O$ (**2**) was determined at $-30°C$ because our preliminary study at room temperature showed a large disorder with respect to the glya ligand bound to the Mn ion. The structure at $-30°C$ still shows a disorder about the glya ligand but the crystallographic data are enough to permit structural discussion.

An ORTEP view of the heptanuclear $\{Mn(glya)\}_6\{Cr(CN)_6\}$ unit of **2** is shown in Fig. 1 together with the atom numbering scheme. Selected bond distances and angles are given in Table 2.

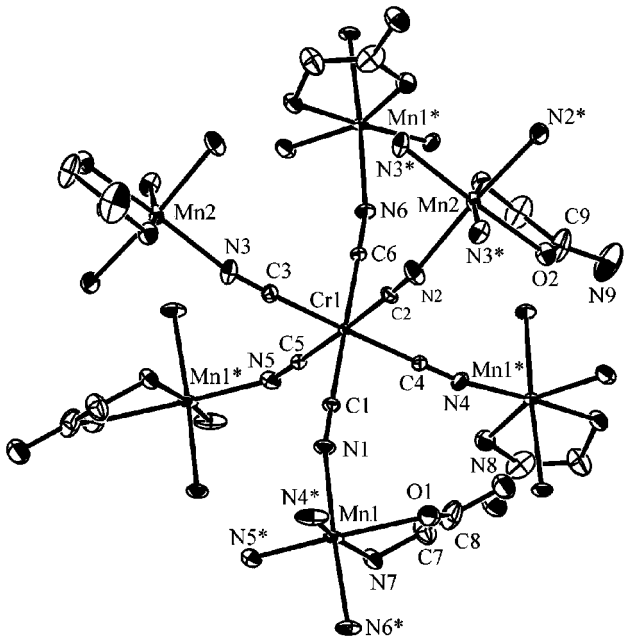

FIG. 1. An ORTEP drawing of the asymmetic unit of **2** with atom numbering scheme.

All the cyanide groups of $[Cr(CN)_6]^{3-}$ are involved in the bridge to the adjacent Mn^{2+} ions. The asymmetric unit consists of one $[Cr(CN)_6]^{3-}$ anion, one $[Mn1(glya)]^{2+}$ cation, one-half of the $[Mn2(glya)]^{2+}$ cation, and 1.25 water molecules. Both Mn1 and Mn2 assume an octahedral environment with one glya ligand and four cyanide nitrogens from adjacent $[Cr(CN)_6]^{3-}$ units (Fig. 1). The Mn2 lies on the glide mirror plane. The X-ray crystallographic study clearly indicates the chelating function of glya. A disorder is seen about Mn1 with respect to the coordination position of glya ligand, as seen in Scheme 1. The occupancies of the two ligand locations, N7-C7-C8(N8)-O1(a) and N7′-C8-C8′(N8′)-O1′(b), are 0.55 and 0.45, respectively. Furthermore, a disorder is seen about Mn2 with respect to the arrangement of the glya ligand (Scheme 2), because of a mirror plane between the two carbon atoms of the glya. That is, the ligand is situated in two different modes, (a) and (b), with the probability of 0.5 and 0.5. The donor atoms of glya are numbered by O2 and O2* and the outer atoms by N9 and N9*, as the result of the symmetry operation ($-x$, y, $\frac{1}{2}-z$), but one of the donor atoms is of course amine nitrogen and one of the outer atoms is absent. The ORTEP view in Fig. 1 is drawn with the location (a) of the glya ligand about Mn 1 and in the situation (a) of the glya ligand about Mn2.

The Cr–C and Mn–N bond distances fall in the range of 2.064(3)–2.072(3) and 2.174(3)–2.242(3) Å, respectively. The Mn–N–C bond angles range from 148.7(3)° to 167.1(3)°.

In the lattice, a three-dimensional network structure is formed by the alternate array of the $[Cr(CN)_6]^{3-}$ and

TABLE 2
Selected Bond Distances and Angles for 1 and 2

	Compound		
	1 (RT)	**1** (−30°C)	**2** (−30°C)
	Bond distances (Å)		
Cr1–C1	2.081(3)	2.076(3)	2.069(3)
Cr1–C2	2.079(3)	2.075(3)	2.073(3)
Cr1–C3	2.076(3)	2.075(3)	2.064(3)
Cr1–C4	2.079(3)	2.084(3)	2.072(3)
Cr1–C5	2.065(3)	2.064(3)	2.064(3)
Cr1–C6	2.075(3)	2.074(3)	2.064(3)
Mn1–N1	2.288(3)	2.287(3)	2.235(3)
Mn1–N4	2.211(3)	2.204(3)	2.178(3)
Mn1–N5	2.208(3)	2.221(3)	2.174(3)
Mn1–N6	2.242(3)	2.241(3)	2.210(3)
Mn2–N2	2.272(3)	2.271(3)	2.242(3)
Mn2–N3	2.204(3)	2.199(3)	2.187(3)
Cr1–C(ave.)	2.076	2.075	2.068
Mn1–N(ave.)	2.237	2.238	2.199
Mn2–N(ave.)	2.238	2.235	2.215
	Bond angles (°)		
Cr1–C1–N1	178.4(3)	178.7(3)	178.7(3)
Cr1–C2–N2	173.2(3)	173.0(3)	175.6(3)
Cr1–C3–N3	177.6(3)	178.4(3)	177.0(3)
Cr1–C4–N4	179.2(3)	179.5(3)	177.3(4)
Cr1–C5–N5	176.2(3)	176.1(3)	176.1(3)
Cr1–C6–N6	176.1(3)	175.8(3)	177.9(3)
Mn1–N1–C1	158.1(3)	157.1(2)	163.2(3)
Mn1–N4–C4	162.1(3)	162.8(3)	164.9(3)
Mn1–N5–C5	145.7(3)	145.1(2)	152.7(3)
Mn1–N6–C6	167.3(3)	167.0(3)	167.1(3)
Mn2–N2–C2	151.8(3)	150.9(3)	148.7(3)
Mn2–N3–C3	163.9(3)	163.4(3)	166.7(3)
Cr1–C–N(ave.)	176.8	176.9	177.1
Mn1–N–C(ave.)	158.3	158.0	162.0
Mn2–N–C(ave.)	157.9	157.2	157.7

$[Mn(glya)]^{2+}$ constituents (Fig. 2). The basic unit is a defective cubane with three Cr atoms, three Mn1 atoms, and one Mn2 atom at the seven corners and eight Cr–CN–Mn edges

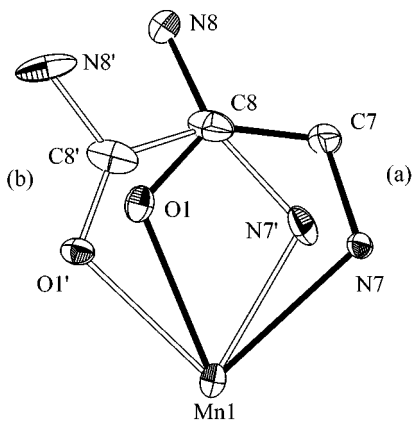

SCHEME 1

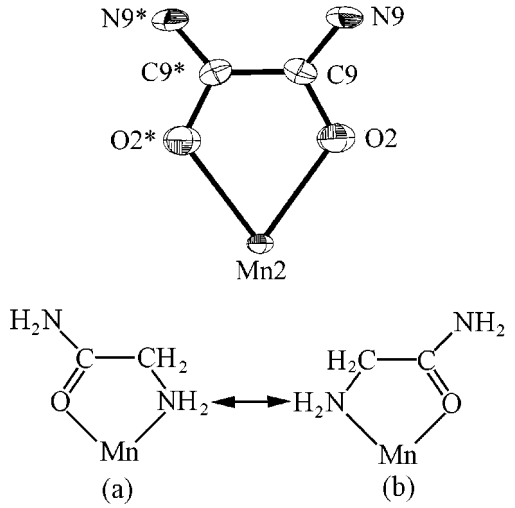

SCHEME 2

(Fig. 3). The shortest Cr1···Mn1, Cr1···Mn2, and Mn1···Mn2 distances are 5.210(1), 5.218(1), and 8.639(1) Å, respectively.

The structure of $[Mn(en)]_3[Cr(CN)_6]_2 \cdot 4H_2O$ (**1**) at room temperature was reported in our preliminary paper (20). It has essentially the same network structure based on a defective cubane unit as found for **2**. In order to compare the

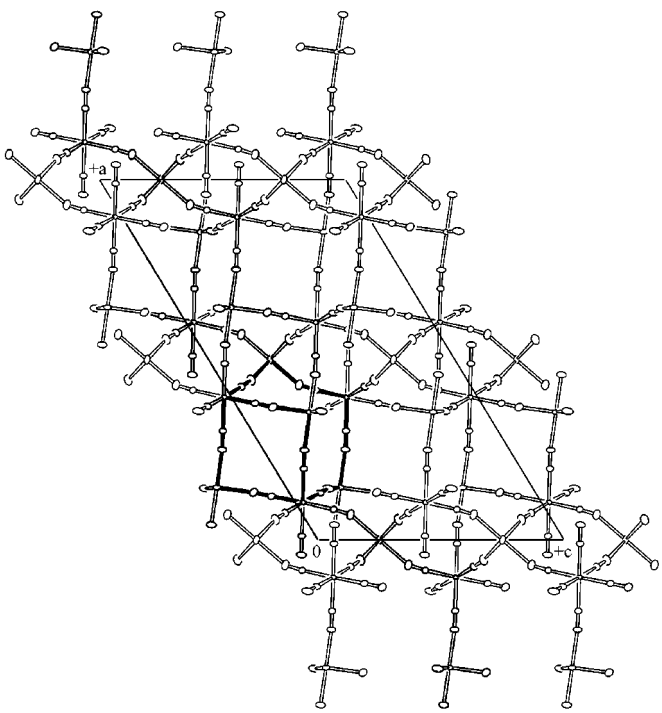

FIG. 2. Projections of the polymeric structure of **2** onto the ac plane (glya and water molecules are omitted for clarity).

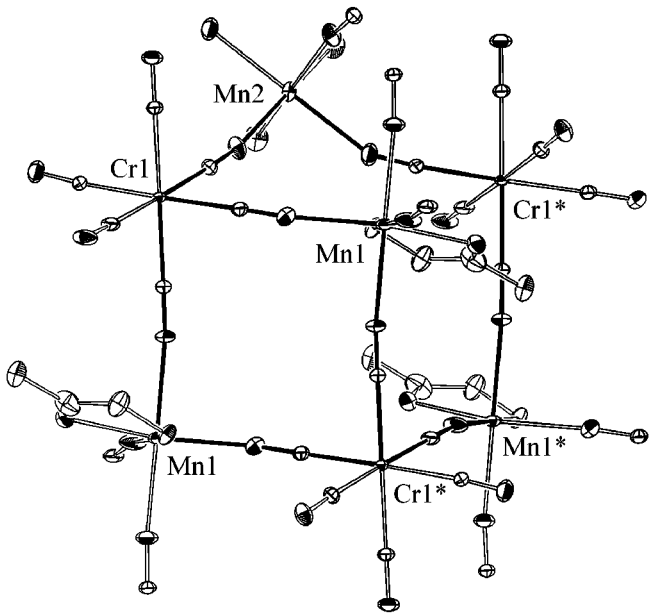

FIG. 3. Defective cubane unit for **2**.

structures of **1** and **2** under the same condition, the crystal structure of **1** has been reexamined at $-30°C$ in this work. An ORTEP view of the heptanuclear $\{Mn(en)\}_6\{Cr(CN)_6\}$ unit of **1** is given in Fig. 4 and the relevant bond distances and angles are included in Table 2. Complex **1** showed no substantial change in bond distances and angles between those at room temperature and those at $-30°C$.

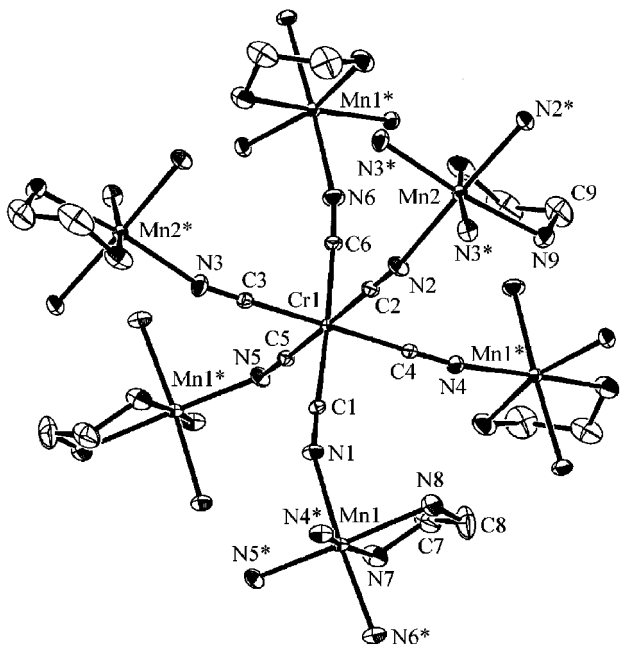

FIG. 4. An ORTEP drawing of the asymmetic unit of **1** with atom numbering scheme.

In comparison of the structures of **1** and **2** at $-30°C$, a noteable difference is seen in the average Mn1–N bond distance and the average Mn–N–C angle. The average Mn1–N bond distance of **1** is 2.238 Å, which is slightly long relative to that of **2** (2.199 Å). The average Mn1–N–C angle of **1** (158.0°) is smaller than that of **2** (162.0°).

MAGNETIC PROPERTIES

$[Mn(en)]_3[Cr(CN)_6]_2 \cdot 4H_2O$ (**1**). The magnetism of **1** was reported in our preliminary paper (20). The results are shown in Fig. 5 in the forms of χ_M vs T and $\chi_M T$ vs T plots (χ_M being the molar magnetic susceptibility per Mn_3Cr_2).

$[Mn(glya)]_3[Cr(CN)_6]_2 \cdot 2.5H_2O$ (**2**). The magnetic behavior of this compound is very similarly to that of **1**. At room temperature the $\chi_M T$ value is 15.22 $cm^3\,K\,mol^{-1}$ (11.04 μ_B) per Mn_3Cr_2, which is smaller than the value expected for isolated two Cr^{III} and three high-spin Mn^{II} ions (16.9 $cm^3\,K\,mol^{-1}$: 11.6 μ_B) (Fig. 6). The $\chi_M T$ value gradually decreased with decreasing temperature to a minimum value of 14.08 $cm^3\,K\,mol^{-1}$ (10.61 μ_B) at 170 K and then increased to a large maximum value of 7544 $cm^3\,K\,mol^{-1}$ (245.7 μ_B) at 56 K. Then the $\chi_M T$ value decreased below this temperature. The χ_M^{-1} vs T plots in the range from 300 to 170 K obey the Curie–Weiss law ($\chi_M^{-1} = C/(T-\theta)$) with a Weiss constant θ of -40.1 K. The negative Weiss constant indicates an intramolecular antiferromagnetic interaction between the adjacent Cr^{III} and Mn^{II} ions through the cyano bridge. The minimum $\chi_M T$ value is close to the spin-only value of 12.38 $cm^3\,K\,mol^{-1}$ (9.95 μ_B) for antiferromagnetically coupled Mn_3Cr_2 ($S = \frac{9}{2}$). The abrupt

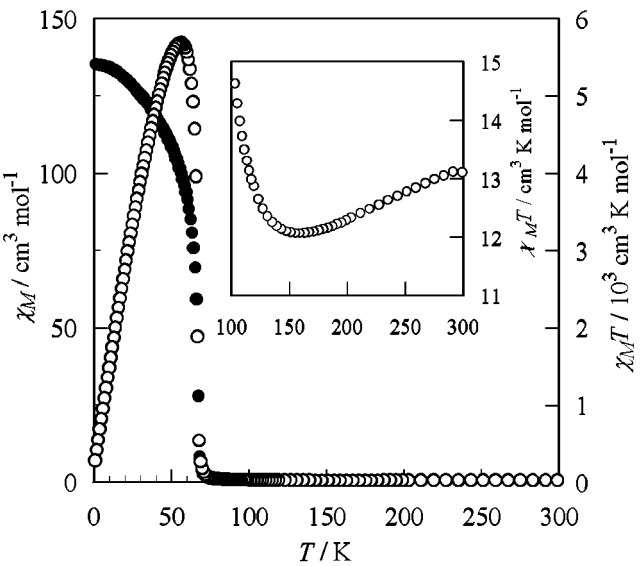

FIG. 5. Temperature dependences of χ_M (●) and $\chi_M T$ (○) for **1**.

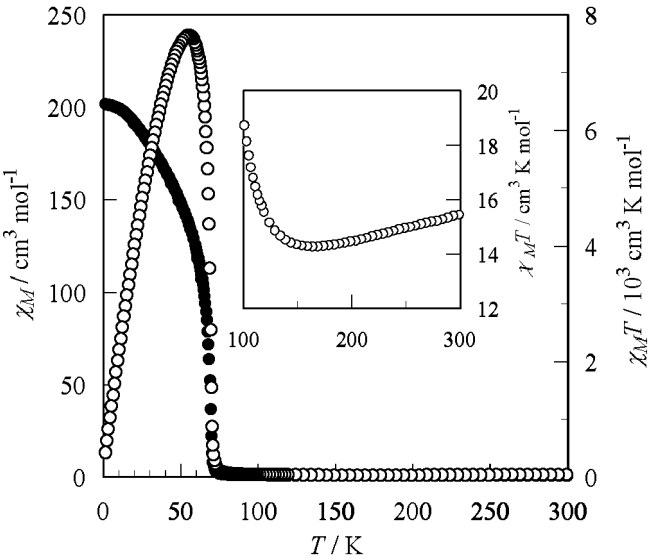

FIG. 6. Temperature dependences of χ_M (●) and $\chi_M T$ (○) for **2**.

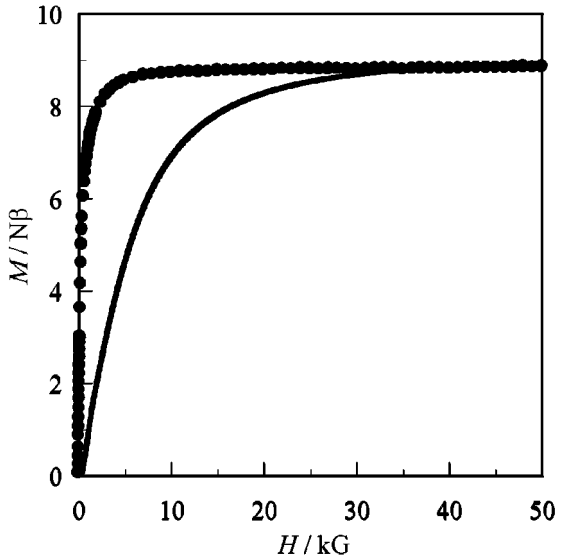

FIG. 8. Field-dependence of the magnetization for **2** at 2 K. The solid line is the Brillouin function for $S = \frac{9}{2}$.

increase in $\chi_M T$ around 70 K suggests the onset of three-dimensional magnetic ordering.

In order to see magnetic ordering in this compound, the temperature dependence of the magnetization M was investigated under an applied field of 5 G (Fig. 7). The field-cooled magnetization (FCM) curve displays a sharp increase of magnetization around 70 K and a tendency of saturation at lower temperature. The remnant magnetization (RM) is observed below 70 K. The zero-field-cooled magnetization (ZFCM) is $756.7\,cm^3\,G\,mol^{-1}$ at 2.0 K, which decreases with increasing temperature. Based on the FCM and ZFCM studies, the T_c of **2** is determined to be 71 K.

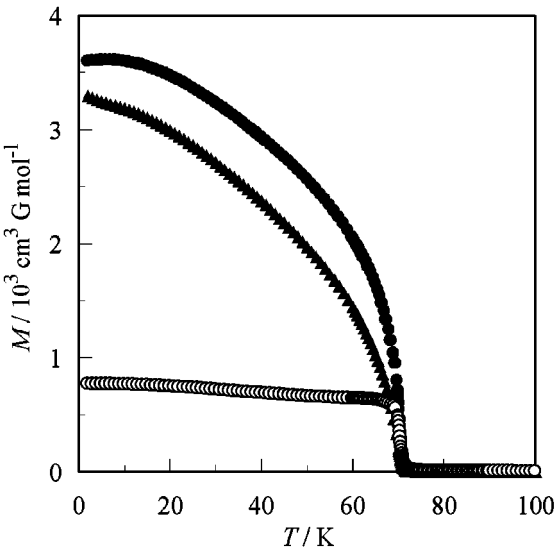

FIG. 7. Temperature dependences of magnetization for **2** under an applied field of 5 G: FCM (●), RM (▲), ZFCM (○).

The field-dependence of magnetization for **2** was measured at 2 K (Fig. 8). The magnetization curve (per Mn_3Cr_2) showed a sharp increase with applied field to reach a saturation value of 8.8 Nβ, which corresponds to the value of $S = \frac{9}{2}$ resulting from antiferromagnetic coupling of three Mn^{II} and two Cr^{III} ions. The Brillouin function for $S = \frac{9}{2}$ is included in Fig. 8, where g is assumed to be 2.0. It is seen that the observed magnetization (per Mn_3Cr_2) is larger than the value expected from the Brillouin function for $S = \frac{9}{2}$ over the field range of 0–35 kG. This is a strong indication of ferrimagnetic ordering in the bulk. The magnetic hysteresis loop of **2** is given in Fig. 9. The behavior observed is typical of soft magnets and supports the saturation of Mn_3Cr_2 at 2 K. The remnant magnetization and coercive field are $1.1 \times 10^4\,cm^3\,G\,mol^{-1}$ and 14 G, respectively. The coercive filed is weak because both of high-spin Mn^{2+} ($S = \frac{5}{2}$) and Cr^{3+} ($S = \frac{3}{2}$) are essentially isotropic and the structure of 3-D network is nearly isotropic.

$Mn_3[Cr(CN)_6]_2 \cdot 12H_2O$ (**3**). This compound shows the χ_M vs T and $\chi_M T$ vs T curves to be very similar to those of **1** and **2**. The $\chi_M T$ value (per Mn_3Cr_2) at room temperature is $13.44\,cm^3\,K\,mol^{-1}$ (10.37 μ_B), which decreased with decreasing temperature to a minimum of $11.84\,cm^3\,K\,mol^{-1}$ (9.73 μ_B) at 140 K, increased to a maximum of $8735\,cm^3\,K\,mol^{-1}$ (264.4 μ_B) at 51 K, and decreased below this temperature (Fig. 10). The ferrimagnetic phase transition temperature was determined to be 63 K based on magnetization studies. This is also a soft magnet with a remnant magnetization of $3.1 \times 10^3\,cm^3\,G\,mol^{-1}$ and a coercive field of 8 G.

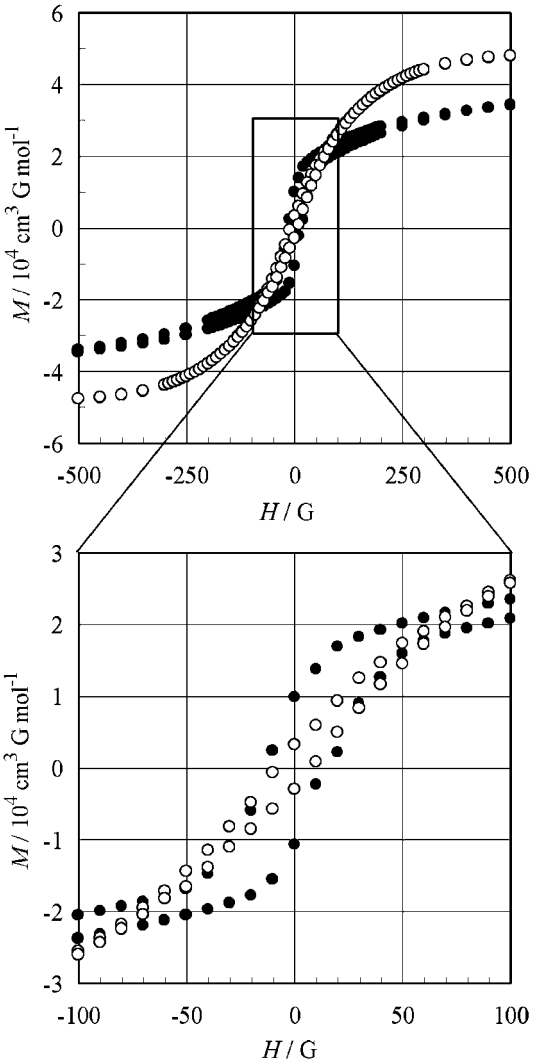

FIG. 9. Magnetic hysteresis loops for **2** (●) and **3**: (○) (top). An extension in the range of $-100 \sim +100$ G is also shown (bottom).

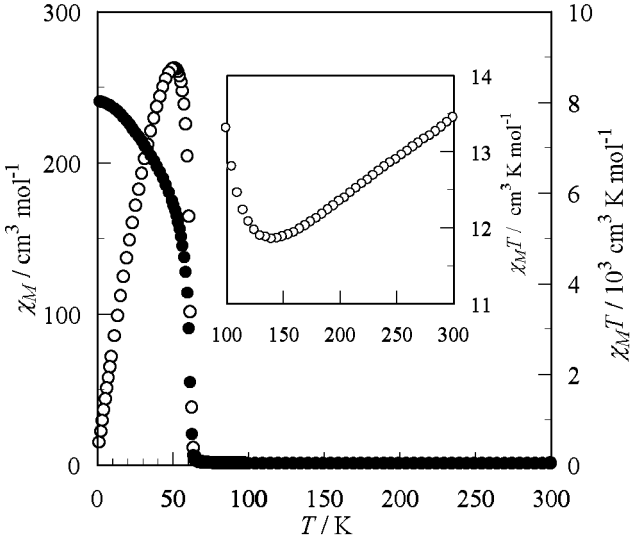

FIG. 10. Temperature dependences of χ_M (●) and $\chi_M T$ (○) for **3**.

Magnetic data for **1–3** are summarized in Table 3. It is seen that **2** has a larger Weiss constant and a higher T_c compared with **1**. These facts mean that **2** shows a stronger antiferromagnetic interaction between the adjacent Cr^{III} and Mn^{II} ions. We have pointed out that the average Mn1–N bond distance is slightly short in **2** relative to **1** and the average Mn1–N–C bond angle is large in **2** relative to **1**. These two effects can explain an enhancement in magnetic interaction between the adjacent Cr^{III} and Mn^{II} ions in **2**.

It is notable that **3** resembles **1** and **2** in magnetic property. The structure of **3** is described as a face-centered three-dimensional network (21), but it must be mentioned that one of the Cr sites in Fig. 11 is not statistically occupied. The geometry about the Mn is octahedral with four cyanide nitrogens from adjacent $[Cr(CN)_6]^{3-}$ molecules and with further coordination of two water molecules. That is, **3** can be formulated as $[Mn(H_2O)_2]_3[Cr(CN)_6]_2 \cdot 6H_2O$, which is equivalent to the present complexes $[Mn(L)]_3[Cr(CN)_6]_2$ (L = en and glya). A correlation is seen between the Weiss constant θ and the magnetic phase transition temperature T_c of **1** and **2**; i.e., the stronger the antiferromagnetic interaction, the higher the magnetic phase transition temperature. However, this correlation does not hold for **3**. Compound **3** shows a stronger antiferromagnetic interaction, judging from the Weiss constant ($\theta = -47.1$ K), but its T_c is lower than that of **1** and **2**. The random lack of Cr^{III} centers in the face-centered cubic lattice can be a reason for the reduction in T_c of **3**. Compound **3** may have a rather small magnetic domain since it is obtained as an amorphous solid, and this can be another reason for the reduction of the T_c.

CONCLUSION

Bimetallic assemblies, $[Mn(en)]_3[Cr(CN)_6]_2 \cdot 4H_2O$ (**1**) and $[Mn(glya)]_3[Cr(CN)_6]_2 \cdot 2.5H_2O$ (**2**), have a three-dimensional network structure based on a defective cubane unit and exhibit a ferrimagnetic ordering at $T_c = 69$ and 71 K, respectively. These assemblies are relevant to a

TABLE 3
Magnetic Properties for 1–3

	1	2	3
Weiss θ (K)	−38.0	−40.1	−47.1
T_c (K)	69	71	63
RM (cm^3 G mol^{-1})	1.2×10^4	1.1×10^4	3.1×10^3
Coercive field H_c (G)	28	14	8
Magnetic nature	Ferrimagnet	Ferrimagnet	Ferrimagnet

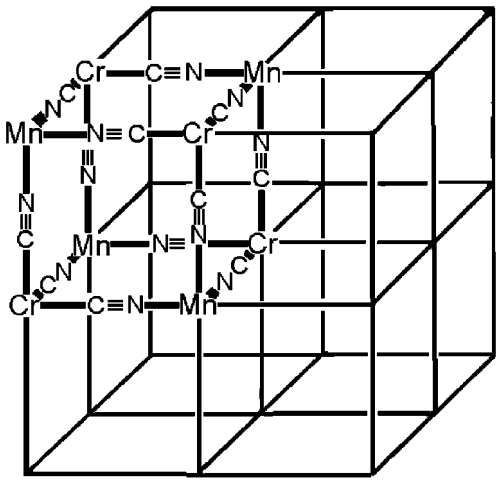

FIG. 11. The network structure of Prussian blue analogue **3**.

Prussian blue analogue, $Mn_3[Cr(CN)_6]_2 \cdot 12H_2O$ (**3**), which is shown in this work to be a ferrimagnet at $T_c = 63$ K.

REFERENCES

1. O. Kahn, "Molecular Magnetism," VCH, Weinhem, Germany, 1993.
2. O. Kahn, *in* "Inorganic Materials," p. 59. Wiley, New York, 1992.
3. O. Kahn, "Structure and Bonding," Vol. 68, Springer-Verlag, Berlin, 1987.
4. O. Kahn, *Adv. Inorg. Chem.* **43,** 179 (1995).
5. D. Gatteschi, O. Kahn, J. S. Miller, and F. Palacio, (Eds), "Molecular Magnetic Material," NATO ASI Series E, Vol. 198. Kluwer Academic, Dordrecht, 1990.
6. M. Turnbull *et al.* (Eds.), "Molecular-Based Magnetic Materials," Symposium Series 644.
7. K. R. Dunbar and R. A. Heintz, *Prog. Inorg. Chem.* **45,** 283 (1997).
8. H. Iwamura and J. S. Miller (Eds.), "Proceeding of Conference on Chemistry and Physics of Molecular-Based Magnetic Materials," *Mol. Cryst. Liq. Cryst.* **232–233** (1993).
9. J. S. Miller and A. J. Epstein, *Angew. Chem. Int. Ed. Engl.* **33,** 385 (1994).
10. J. S. Miller and A. J. Epstein, "Designer Magnets," C&EN Special Report, October, 30, 1995.
11. D. Gatteschi, *Adv. Mat.* **6,** 635 (1994).
12. W. D. Griebler and D. Z. Babel, *Naturforsch. B* **37,** 832 (1982).
13. V. Gadet, T. Mallah, I. Castro, and M. Verdauguer *J. Am. Chem. Soc.* **114,** 9213 (1992)
14. W. R. Entley and G. S. Griolani, *Science* **268,** 397 (1995).
15. S. Mallah, S. Thiebaut, M. Verdauguer, and P. Veillet, *Science* **262,** 1554 (1993).
16. S. Ferlay, T. Mallah, R. Ouahes, P. Veillet, and M. Verdauguer, *Nature* **378,** 701 (1995).
17. W. R. Entley and G. S. Girolani, *Inorg. Chem.* **33,** 5165 (1994).
18. (a) M. Ohba, H. Ōkawa, N. Fukita, and Y. Hashimoto, *J. Am. Chem. Soc.* **119,** 1011 (1997). (b) M. Ohba and H. Ōkawa, *Mol. Cryst. Liq. Cryst.* **286,** 101 (1996). (c) M. Ohba, H. Ōkawa, T. Ito, and A. Ohto, *J. Chem. Soc. Chem. Soc.* **15,** 1545 (1995). (d) M. Ohba, N. Maruono, H. Ōkawa, T. Enoki, and J. M. Latour, *J. Am. Chem. Soc.* **116,** 11566 (1994). (e) M. Ohba, N. Fukita, and J. Ōkawa, *J. Chem. Soc. Dalton Trans.* 1733 (1997). (f) M. Ohba, N. Usuki, N. Fukita, and H. Ōkawa, *Inorg. Chem.* 3349 (1998). (g) M. Ohba and H. Ōkawa, *Coord. Chem. Rev.* **198,** 313 (2000).
19. N. Fukita, M. Ohba, H. Ōkawa, K. Matsuda, and H. Iwamura, *Inorg. Chem.* **37,** 842 (1998).
20. M. Ohba, N. Usuki, N. Fukita, and H. Ōkawa, *Angew. Chem. Int. Ed. Engl.* **38,** 1795 (1999).
21. H. U. Güdel, H. Stucki, and A. Ludi, *Inorg. Chim. Acta* **7,** 121 (1973).
22. teXsan: Crystal Structure Analysis Package, Molecular Structure Corporation, 1985, 1992.